

## RESEARCH ARTICLE

# A comparative study of CARE 2D and N2V 2D for tissue-specific denoising in second harmonic generation imaging

Arash Aghigh<sup>1</sup>  | Gaëtan Jargot<sup>1</sup> | Charlotte Zaouter<sup>2</sup> | Samuel E. J. Preston<sup>3,4</sup> | Melika Saadat Mohammadi<sup>1</sup>  | Heide Ibrahim<sup>1</sup> | Sonia V. Del Rincón<sup>3,4</sup> | Kessen Patten<sup>2</sup> | François Légaré<sup>1</sup>

<sup>1</sup>Centre Énergie Matériaux Télécommunications, Institut National de la Recherche Scientifique, Varennes, Québec, Canada

<sup>2</sup>Armand-Frappier Santé Biotechnologie Research Centre, Laval, Québec, Canada

<sup>3</sup>Department of Experimental Medicine, Faculty of Medicine, McGill University, Montréal, Québec, Canada

<sup>4</sup>Gerald Bronfman Department of Oncology, Segal Cancer Centre, Lady Davis Institute and Jewish General Hospital, McGill University, Montréal, Québec, Canada

## Correspondence

Arash Aghigh, Centre Énergie Matériaux Télécommunications, Institut National de la Recherche Scientifique, Varennes, Québec, Canada.

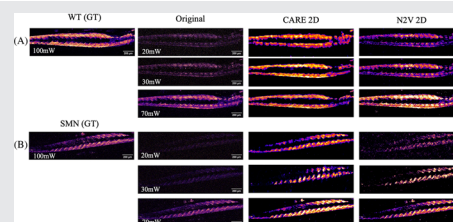
Email: [arash.aghigh@inrs.ca](mailto:arash.aghigh@inrs.ca)

## Funding information

the Natural Sciences and Engineering Research Council of Canada, the New Frontiers Research Fund; Fonds de recherche du Québec - Nature et technologies; Canadian Cancer Society, Grant/Award Number: 707140; NSERC CREATE program; Epstein Fellowship in Women's Health (Faculty of Medicine, McGill University); Fonds de Recherche du Québec - Santé; Canada Foundation for Innovation

## Abstract

This study explored the application of deep learning in second harmonic generation (SHG) microscopy, a rapidly growing area. This study focuses on the impact of glycerol concentration on image noise in SHG microscopy and compares two image restoration techniques: Noise-to-Void 2D (N2V 2D, no reference image restoration) and content-aware image restoration (CARE 2D, full reference image restoration). We demonstrated that N2V 2D effectively restored the images affected by high glycerol concentrations. To reduce sample exposure and damage, this study further addresses low-power SHG imaging by reducing the laser power by 70% using deep learning techniques. CARE 2D excels in preserving detailed structures, whereas N2V 2D maintains natural muscle structure. This study highlights the strengths and limitations of these models in specific SHG microscopy applications, offering valuable insights and potential advancements in the field.



## KEYWORDS

deep learning, denoising, ECM imaging, image restoration, myosin imaging, SHG microscopy

This is an open access article under the terms of the [Creative Commons Attribution-NonCommercial License](https://creativecommons.org/licenses/by-nc/4.0/), which permits use, distribution and reproduction in any medium, provided the original work is properly cited and is not used for commercial purposes.

© 2024 The Authors. *Journal of Biophotonics* published by Wiley-VCH GmbH.

## 1 | INTRODUCTION

Second harmonic generation (SHG) microscopy is a powerful nonlinear optical microscopy technique that has been successfully used in medical and nonmedical imaging for years [1–4]. Image quality in microscopy crucially depends on the signal-to-noise ratio (SNR), which is the ratio of signal intensity to noise. Factors such as laser power, exposure time, and the sample itself play crucial roles in influencing the SNR. It is well known that an increase in laser power while enhancing the SHG signal risks thermal damage to the sample [5]. For example, increasing the laser power can produce a higher SHG signal but may cause thermal damage to a sample [6–8]. Therefore, finding the optimal tradeoff between the laser power and achieving an acceptable SNR (i.e., having the sample structure visible with noise present) is critical. In addition to the instrumental parameters, sample type is another critical criterion that can affect the SNR in SHG microscopy. While we observed strong SHG signals from collagen-rich tissues [9] and skeletal muscles [10], some samples, such as microtubules, inherently have a weak SHG signal [11]. Samples with a lower SHG signal have a low SNR, and their structure can be buried under background noise, depending on the experimental conditions.

Within the evolving landscape of SHG microscopy, deep learning is a transformative tool for classification, segmentation, and image restoration. We provide ample examples of different studies focusing on different applications. In [12] a classification application, a method for diagnosing ovarian cancer during surgery using SHG imaging and deep learning techniques is introduced. By training a convolutional neural network (CNN) on a vast dataset of SHG images, the system can differentiate between normal, benign, and malignant ovarian tissues with 99.7% accuracy. In [13] a segmentation application, the effectiveness of a U-Net CNN for improving the segmentation of collagen fibers in SHG images was demonstrated. The CNN successfully addressed the challenges posed by varying the SHG image intensity across the depths. This method consistently outperformed the traditional thresholding techniques, particularly in deeper tissue sections. Although not focused solely on SHG, [14] compared different denoising techniques to improve the quality of nonlinear multimodal images in head and neck tissue analysis. In this study, traditional methods (e.g., median filter and Gerchberg-Saxton), established deep learning networks (e.g., DnCNN), and innovative networks (e.g., Noise2Noise, MIRNet, and incSRCNN), specifically focusing on their ability to reduce noise while preserving critical image details. In another study, researchers introduced a fast large-area multiphoton exoscope (FLAME) for imaging human

skin [15]. The FLAME system incorporates a deep-learning-based image restoration technique using a content-aware image restoration (CARE) model network. This approach improves the quality of the images captured by the system. These studies demonstrate the broad potential of deep learning in SHG microscopy. However, tissue-specific variations in signal intensity and the impact of preparation techniques introduce unique challenges for image restoration in SHG. The application of deep learning techniques specifically tailored for improving low-SNR SHG imaging has not been extensively explored. This gap presents a unique opportunity for research aimed at addressing the specific challenges associated with SHG microscopy, particularly in tissue-specific imaging under low-SNR conditions.

Image restoration enhances the image quality by eliminating noise, artifacts, and other distortions [16, 17] without creating hallucinations (generation of visual structures that are not based on the actual information available in the input image [18]). Deep learning image restoration has been successfully applied to fluorescence- [16, 17], super-resolution- [19, 20], structured illumination- [21], and electron microscopy [22, 23]. It has also been applied to multiphoton microscopy [14, 15].

Three of the many different types of available image restoration techniques to remove noise are noise-to-ground truth (N2GT) [16], noise-to-noise (N2N) [24], and noise-to-void (N2V) [25]. N2GT refers to the removal of noise from an image by comparison to a reference image, also known as the ground truth image, which is assumed to be noise-free and used as a guide in the denoising process [16]. The availability of GT images is a limitation of this method [16, 25]. N2N refers to removing noise from an image (low SNR) by comparing it to another noisy image (high SNR) rather than to a GT image [24, 26]. This method is more widely applicable because it does not require a noise-free image [24]. One model in this category is the CARE model based on the U-net CNN [27]. It is among the models that require high- and low-SNR image pairs to perform image restoration [26]. N2V refers to removing noise from an image by creating a deep neural network to learn the statistical properties of the noise and the signal within one image [25]. Unlike previous methods, which require an image pair, this method does not require such a requirement and uses a single noisy image for training.

Common methods for evaluating denoised image quality include the Structural Similarity Index Metric (SSIM) and peak SNR (PSNR) to ensure hallucination-free image generation. Both metrics were used to compare the similarities between the original and processed images. The PSNR is calculated by taking the ratio of the

maximum signal to the mean squared error between the original and processed images. The higher the PSNR value, the higher the quality of the processed image. The SSIM is a metric that uses structural and textural information. It compares structural information by measuring the similarities between the original and processed images' mean value, standard deviation, and cross-covariance [28]. The value of SSIM ranges between 0 and 1, where 1 indicates perfect similarity, 0 indicates poor similarity, and  $-1$  indicates perfect anticorrelation. The SSIM and PSNR metrics have different sensitivities to image degradation [29–31].

Our study uniquely addressed the tissue-specific imaging challenges of collagen and myosin within the SHG microscopy domain, investigating the effects of glycerol concentration on zebrafish fixation [32], and exploring low-laser-power imaging across diverse biological specimens, including muscle tissues from two zebrafish strains, and the intricate extracellular matrix barrier of tumor-bearing mouse mammary glands. This focus on tissue specificity coupled with our tailored application of advanced denoising techniques sets our research apart. By applying CARE 2D and N2V 2D in such a targeted manner and evaluating their effectiveness with mSSIM and PSNR metrics, our study not only highlights the adaptability and efficacy of deep learning for SHG microscopy but also emphasizes its potential for tissue-specific imaging under low-SNR conditions. This approach ensures the preservation of structural details and effective noise elimination, contributing significantly to the advancement of the field and opening new avenues for precision in biomedical imaging.

## 2 | METHODOLOGY

### 2.1 | Tissue preparation

Adult wild-type (WT) and mutant survival motor neuron (*smn*) zebrafish (*Danio rerio*) were maintained at 28°C under a light/dark cycle of 12/12 h according to the Westerfield zebrafish book [32]. Embryos were raised at 28.5°C, collected, and staged as previously described [33]. All animal experiments were performed in compliance with the Canadian Council for Animal Care guidelines and approved by the INRS-LNBE ethics committee. Genotyping of *smn* larvae was performed by high-resolution melting analysis using genomic DNA extracted by a non-invasive genotyping protocol [34]. Larval (5-day postfertilization) *smn*<sup>-/-</sup> (homozygous) and WT zebrafish were fixed in 4% paraformaldehyde overnight at 4°C. After fixation, the larvae were rinsed several times (1 h) with PBS-Tween and mounted on slides in 50%–100% glycerol,

and finally, their muscles were imaged using SHG microscopy.

Female BALB/c mice were purchased from Charles River Laboratories. All animal experiments were conducted according to the regulations established by the Canadian Council of Animal Care under protocols approved by the McGill University Animal Care and Use Committee. The murine tumor-bearing samples used in this study were derived from orthotopic injection of 4T1 cells into nulliparous mice. 4T1 cells were provided by Dr. Peter Siegel (McGill University) and cultured in DMEM (Wisent) supplemented with 10% FBS and antibiotics. Cells were maintained at a low passage number prior to use. For both models,  $1 \times 10^5$  cells were injected into the fourth mammary fat pad and tumors were allowed to grow for 2 weeks. Fourteen days postinjection, the mice were euthanized, and the primary tumors and surrounding stroma were removed. The samples were fixed in 10% Neutral Buffered Formalin (VWR International LLC) for 48 h at 4°C, after which they were stored in 70% ethanol. Following fixation, naïve and tumor-bearing mammary glands were embedded in paraffin and serially sectioned (5  $\mu$ m thickness). The slides were deparaffinized and rehydrated by submersion in three rounds of xylene, two rounds of 100% ethanol, one round of 95% ethanol, and one round of 70% ethanol (5 min per round). The rehydrated slides were then rinsed for 5 min in distilled water. Coverslips (VWR International LLC, No. 1) were mounted onto slides using the Permount mounting medium (Fisher). The slides were allowed to dry overnight before downstream microscopy.

### 2.2 | SHG imaging setup

SHG microscopy was performed using a custom-stage inverted scanning microscope, as shown in Figure 1. A mode-locked Ti:Sa laser (Tsunami, Spectra-Physics) pumped by a 12 W Millennia Pro laser (Spectra-Physics) was used. This laser delivered pulses of approximately 810 nm with 150 fs pulse duration, at 80 MHz repetition rate with an average power of 2.5 W. For power control, a half-wave plate and a Glan-Thompson polarizer were used to adjust the average power from 20 to 110 mW (0.25–1.38 nJ pulse energy). Given the size of the samples for imaging, sample scanning was performed using a high-speed motorized XY scanning stage (MLS203, Newton, NJ). The focus was adjusted coarsely and finely by using mechanical and piezoelectric motors (PI Nano-Z, USA). An air objective (UplanSApo 20X, NA 0.75, Olympus, Japan) was used for the illumination. A condenser was used to collect the SHG signal of the sample, which was detected using a photomultiplier tube (R6357,

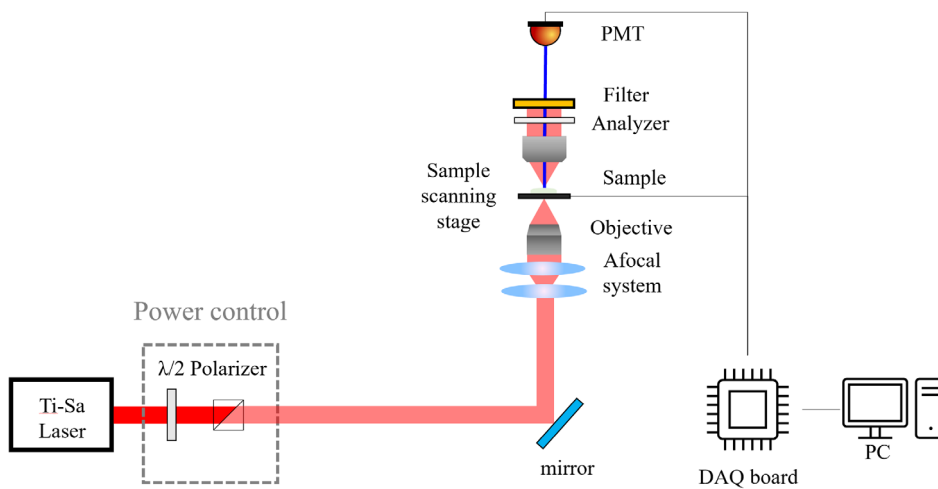


**FIGURE 1** Layout of the SHG inverted microscope. The microscope and data acquisition were performed using a unified custom Python program.

Hamamatsu Photonics) set at 800 V. The SHG signal was isolated using two spectral filters that were placed before the photomultiplier. A short-pass filter that blocks any wavelength higher than 720 nm (i.e., the input fundamental laser light) was employed with a bandpass filter centered at 405 nm to filter out any residual input light. A multichannel I/O board (National Instruments) and custom-written Python program were used for signal acquisition and synchronization. Given the sample size and acceleration and deceleration times of the motorized scanning stage, each SHG image had an acquisition time of a few minutes. Raw data were visualized using Fiji-ImageJ software (NIH, USA).

### 2.3 | Image restoration using CARE 2D and N2V 2D

Image restoration was performed using the CARE 2D and N2V 2D models. The models were run using the Jupyter notebook provided by the ZeroCostDL4Mic toolbox [35] on Google Colaboratory. For the mammary gland cancer samples, the N2V 2D model was trained from scratch for 2000 epochs on 392 image patches (image dimensions: [500,500], patch size: [64,64]) with a batch size of 128. The CARE 2D model was trained from scratch for 300 epochs on 200 image patches (image dimensions: [500,500], patch size: [64,64]) with a batch size of 16. The reason for having different numbers of training epochs is to compensate for the limited amount of available reference data and allow the N2V 2D model to train for a longer time compared to the CARE 2D model. This extended training duration is essential for N2V 2D, as it leverages self-supervised learning, relying on inherent noise patterns within the data to improve its performance, which necessitates additional training to effectively model and remove noise. For the zebrafish

samples, the N2V 2D model was trained from scratch for 2000 epochs on 800 image patches (image dimensions: [333,1333], patch size: [64,64]) with a batch size of 128. The CARE 2D model was trained from scratch for 300 epochs on 50 image patches (image dimensions: [333,1333], patch size: [64,64]) with a batch size of 16. Data augmentation was used in its default setting in all cases, and for CARE 2D, the Augmentor was used [36]. The essential Python packages include TensorFlow, Keras, CSBdeep, NumPy, and Cuda. The training was accelerated using a Tesla T4 GPU on Google servers.

## 3 | RESULTS AND DISCUSSION

### 3.1 | Fixation: Evaluation of the dependence of noise as a function of glycerol content

Sample preparation is essential for any microscopic method [37]. The chemicals used in fixation can cause image deterioration in SHG microscopy for some samples, such as microtubules [11]. Moreover, there is no universal protocol for fixation and each tissue has a unique method [3]. Three glycerol concentrations were tested to determine the best fixation composition for the SHG imaging of zebrafish samples. Because of the different locations of the samples, different image sizes were obtained with a laser input power of 75 mW at the focus of the microscope objective. Figure 2 depicts the different samples with different glycerol concentrations that were imaged and their denoised counterparts.

Our study found a correlation between glycerol concentration and noise in the final image; the lower the glycerol concentration, the better the image quality. The minimum amount of glycerol that could be used without disturbing the fixation process is 50%. We then

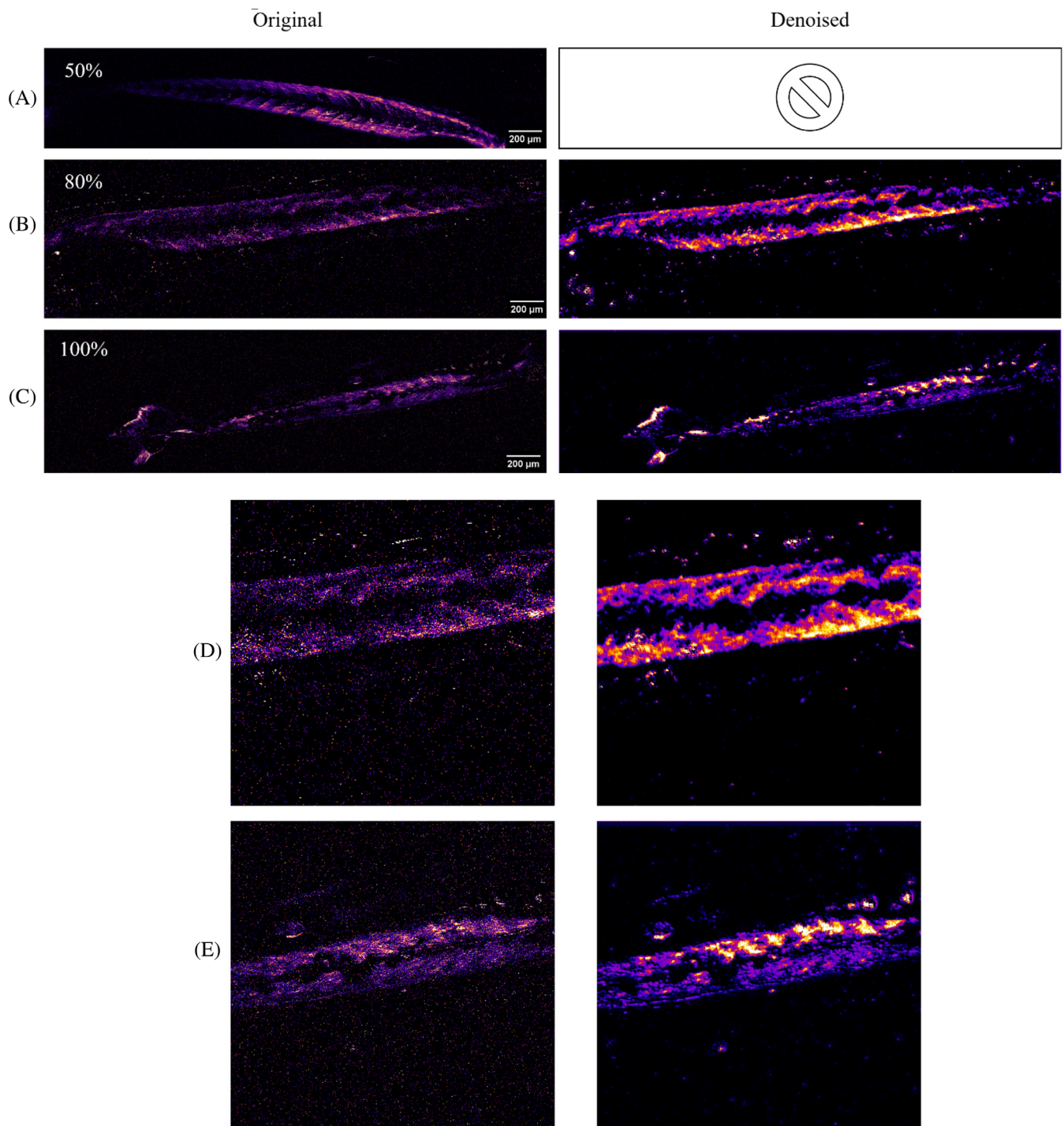


**FIGURE 2** Left column: SHG images of different zebrafish samples with (a) 50%, (b) 80%, and (c) 100% glycerol concentration in their fixation alongside zoom in (d, e) for samples (b) and (c), respectively. As the glycerol content in the fixation increases, the SHG image becomes noisier. Right column: Denoising based on the N2V 2D method was performed for 80% and 100% glycerol content, and it was unnecessary for 50% concentration.

tested N2V 2D and CARE 2D to denoise images with higher glycerol concentrations. The CARE 2D model for these samples resulted in overfitting [38, 39] during model training and was not applicable. N2V 2D could successfully restore images in both high-concentration glycerol cases and retrieve the structural information of

the fish muscle, as shown in the right column. Given the amount of time and effort required for sample preparation, in some cases, deep learning tools can be used to restore the image quality instead of restarting the sample preparation to determine the perfect chemical composition and physical location of the sample. The

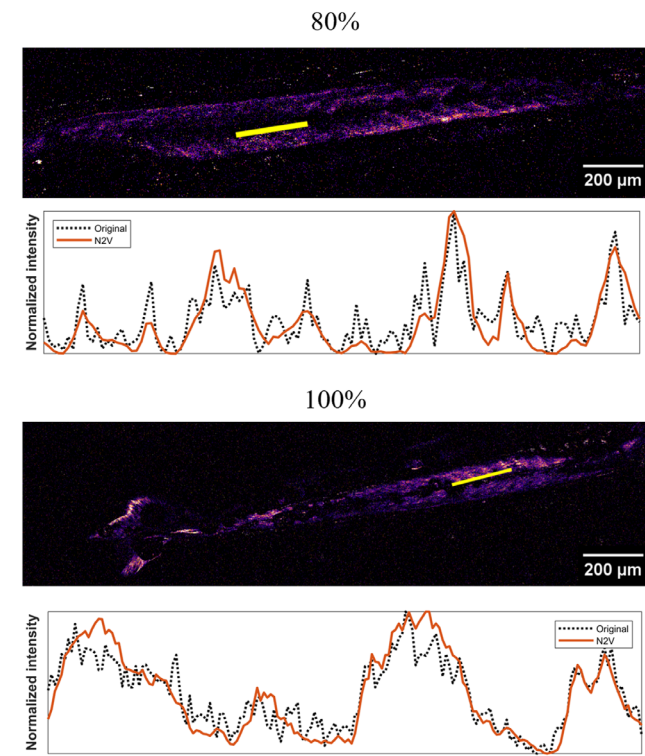


**FIGURE 3** The intensity profile of 80% and 100% glycerol content fixation was imaged at 75 mW input laser power for the original (black dotted line) and denoised (red solid line) images.

intensity profiles for 80% and 100% glycerol are shown in Figure 3.

For the intensity profile, we plotted the intensity values of the pixels along the yellow line, as shown in Figure 3. From this figure, we can see that for 80% glycerol, the model enhances the contrast of the image. A comparison with the original signal shows that it follows the same overall intensity pattern as a cleaner (omission of noise) signal. For 100% glycerol, the signal fits the intensity profile of the original, but without noisy spikes. Therefore, in cases where the chemicals in the fixation cause noise in the sample images (glycerol content in our case), N2V 2D is a perfect model for image restoration, given that sample preparation and fixation are time consuming. Moreover, it can reduce the number of animals that need to be sacrificed for sample preparation.

### 3.2 | CARE 2D and N2V 2D models on tumor-bearing mammary glands

We created low- and high-SNR SHG images by varying the laser input power at the focus of the objective lens. Using this approach, we obtained a less noisy (ground truth) measurement with 110 mW of input laser power at the focus of the microscope objective. The CARE 2D and

N2V 2D models were applied to SHG images of the boundary of a murine mammary gland tumor, and Figure 4 shows the results generated by these models.

The original image in Figure 4B shows an extremely poor SNR. Using the CARE 2D model, we can still extract structural information about the boundary. However, this method leads to “hallucinations,” in which a structure is created within the tumor area that is absent. Moreover, the N2V 2D model could not provide a clean image. The original image in Figure 4C presents a low SNR; in this case, CARE 2D provides the complete structure of the collagen boundary around the tumor, with some fine details being blurred. N2V 2D can only denoise the bright spots in the image; a silhouette of the boundary is visible but not usable for analysis. The original image in Figure 4D presents good SNR. Here, CARE 2D enhances the crispness of the SHG images obtained, and we observe an improvement in the details and sharpness of the image. The contrast was also improved, as shown by the intricate details of the collagen boundary structure. In this case, N2V 2D also performs well, and the details of the collagen boundary structure are visible and patchy, with point-like bright spots where the SHG signal is strong. The mSSIM and PSNR parameters of the results are summarized in Table 1.

For the CARE 2D model, we observed a negligible improvement in SSIM between the original and denoised images in the 20 mW case, and the PSNR remained the same. For 30 mW, we see the highest improvement, as the mSSIM metric almost doubles between the original and denoised images, while the PSNR has a substantial boost. For 70 mW, although some improvement in mSSIM and PSNR is observed, it is not as drastic as in the case of 30 mW. For the N2V 2D model, we see a substantial improvement in the mSSIM for the 30 mW case, but the PSNR decreases. We can see that the image did not improve in terms of details and structural information with visual inspection. For the 70 mW case, the mSSIM and PSNR of the denoised image are lower than those of the original image, and a visual inspection reveals the patchy and disjointed nature of the denoised image. In addition to the quality control metrics, we also considered a random region of interest and measured the performance of the models by plotting the intensity profile in Figure 4.

For 20 mW (see Figure 5A,B), we can see that the original intensity profile contains many noise spikes, while the denoised model can smoothen these spikes and provide a profile closer to the ground truth image with overshoots in some places. CARE 2D provides a good fit that smoothenes out the original signal and remains close to the ground truth intensity profile, but with some peaks that are smoothed. At 30 mW (see Figure 5A,C), the performance of CARE outshines N2V

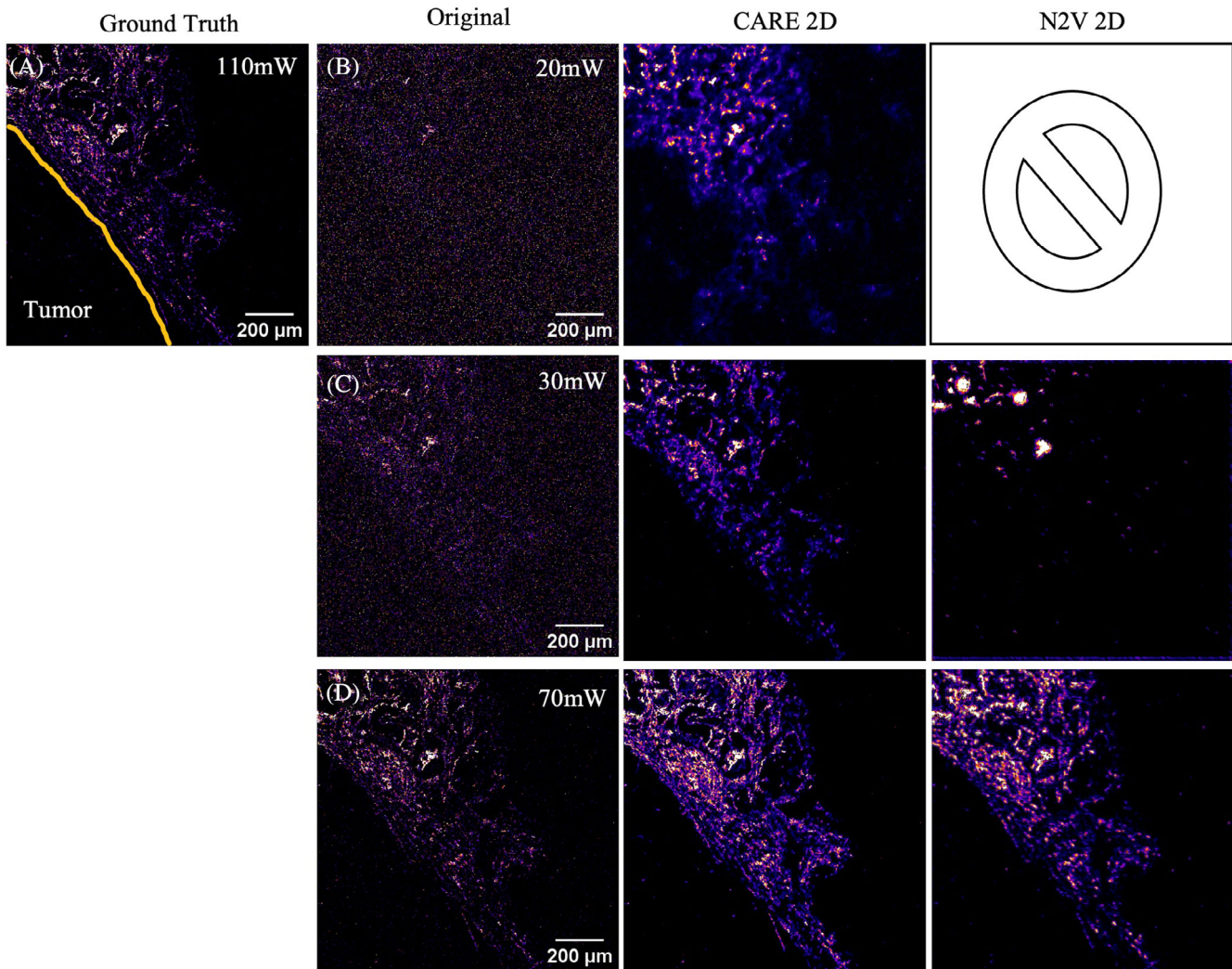


**FIGURE 4** CARE 2D and N2V 2D models were applied to the collagen structure at the tumor boundary of a tumor-bearing mammary gland. (a) The reference “ground-truth image is used to denoise the images using CARE 2D and for visual comparison. (b, c) present low SNR SHG images, and (d) presents a high SNR SHG image.

**TABLE 1** mSSIM and PSNR metric for CARE 2D and N2V 2D model applied to the SHG imaging of the boundary of tumor-bearing mammary glands.

Model	CARE 2D			N2V 2D	
	20	30	70	30	70
Original vs. GT mSSIM	0.33	0.38	0.85	0.38	0.85
Denoised vs. GT mSSIM	0.34	0.79	0.89	0.55	0.80
Original vs. GT PSNR (dB)	20.83	23.12	29.73	23.12	29.74
Denoised vs. GT PSNR (dB)	20.83	27.57	30.01	21.81	24.44

2D, and we can see that the intensity profile for CARE resembles the ground truth image's intensity profile. N2V 2D, however, only provides some spots with high intensities in both the region of interest and the intensity profile. At 70 mW (see Figure 5A,D), the performances of both models are comparable, and they both provide an intensity profile that fits close to the ground

truth image. Both models exhibited enhanced contrast, characterized by more pronounced peaks and deeper valleys in the denoised images, indicating a clearer differentiation between features.

Overall, we conclude that the CARE 2D model performs better than N2V 2D because of the additional information input available during training in the form of a

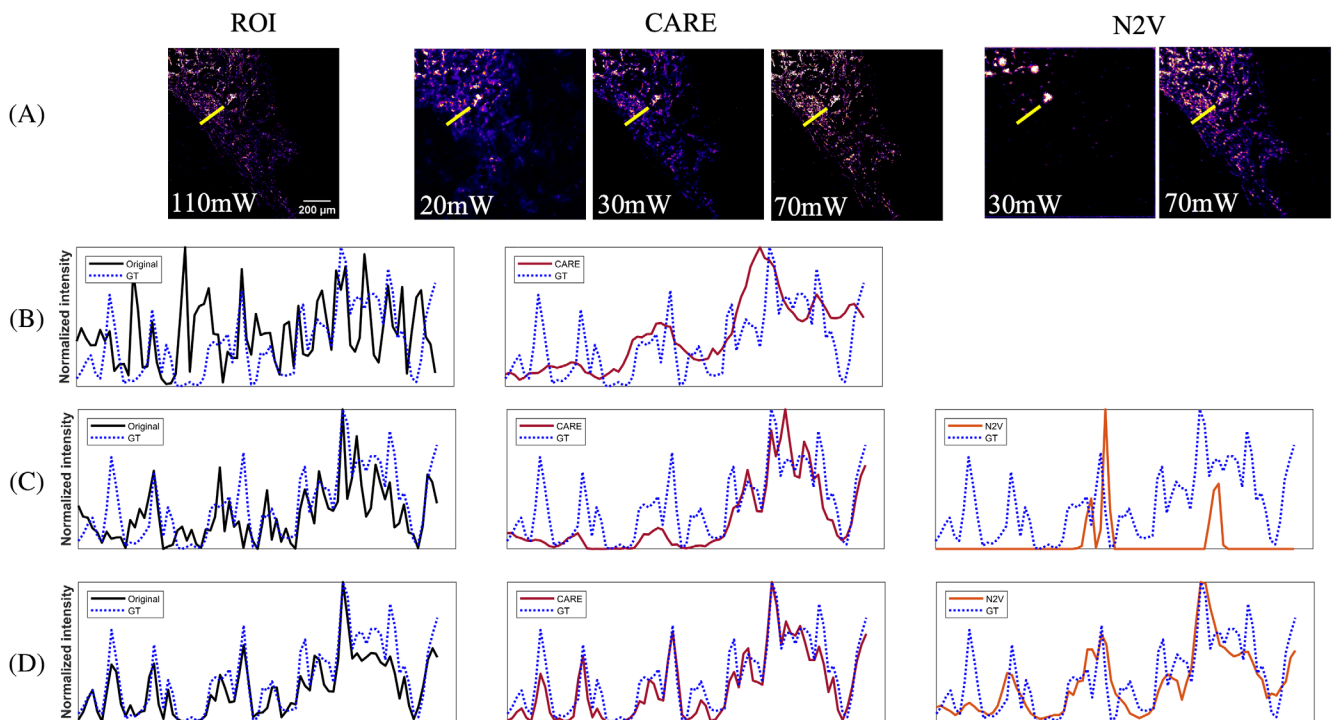


**FIGURE 5** Intensity profile of a random region of interest (ROI) at the tumor boundary. where (a) represents the visual representation of the ROI for the different power profiles. The intensity profiles for the ROIs can be seen at 20 mW (b), 30 mW (c), and 70 mW (d). The legends correspond to the original structure (black solid line), GT (blue dotted line), CARE (red solid line), and N2V (orange solid line).

ground-truth image. Nevertheless, in the higher SNR cases, the performances of both models were comparable. Therefore, for exceptionally low SNR cases, CARE 2D is a better choice for denoising the detailed structures, especially in the case demonstrated in this section. For higher SNR cases, both models performed well in denoising the image and providing structural details. In the next section, we examine the performance of these models in the case of myosin, another common biological structure imaged using SHG microscopy.

### 3.3 | CARE 2D and N2V 2D for denoising zebrafish muscle structures

The CARE 2D and N2V 2D models were also applied to two zebrafish strains: WT and *smn*<sup>-/-</sup>. The results are shown in Figure 6.

For WT samples at 20 and 30 mW, the predicted images appear to have improved in terms of pure SHG intensity when compared to their original counterparts. However, there was also a noticeable loss of detail in muscle structure. The CARE 2D smoothens the distinct muscle structure, resulting in a more uniform appearance. In terms of muscle structure preservation, N2V 2D outperformed CARE 2D in all the cases. While some muscle structure distinctions can still be seen at 70 mW

with CARE 2D, most of them have been smoothed out. However, N2V 2D does not deliver the same SHG intensity restoration as CARE 2D, except at 70 mW. Despite this, N2V 2D is preferred in muscle structure studies as it focuses on the morphology and structural changes in different samples, as well as in intensity.

Our study also aimed to evaluate the performance of the CARE 2D and N2V 2D models for the *smn*<sup>-/-</sup> fish, which has a lower SHG intensity than the WT samples. In low-power cases, both models performed poorly with patchy and choppy muscle representations, although CARE 2D showed better performance than N2V 2D at 20 and 30 mW. At 70 mW, both models performed comparably, with CARE 2D delivering more SHG intensity, whereas N2V 2D preserved more muscle details. Surprisingly, N2V 2D outperformed CARE 2D in terms of muscle detail preservation and denoising of zebrafish muscle structures, even though it did not have a reference image for training. Therefore, N2V 2D is the preferred model for these applications. Based on Figure 6, CARE 2D matches the GT image intensity for WT samples at low power but at the cost of smoothing out most of the signal. N2V 2D, however, provides an intensity profile that is closer to the original image in terms of preserving details. At 70 mW, CARE 2D provides the same intensity value as the original image while reducing noise spikes, and N2V 2D again falls in the middle between the CARE 2D

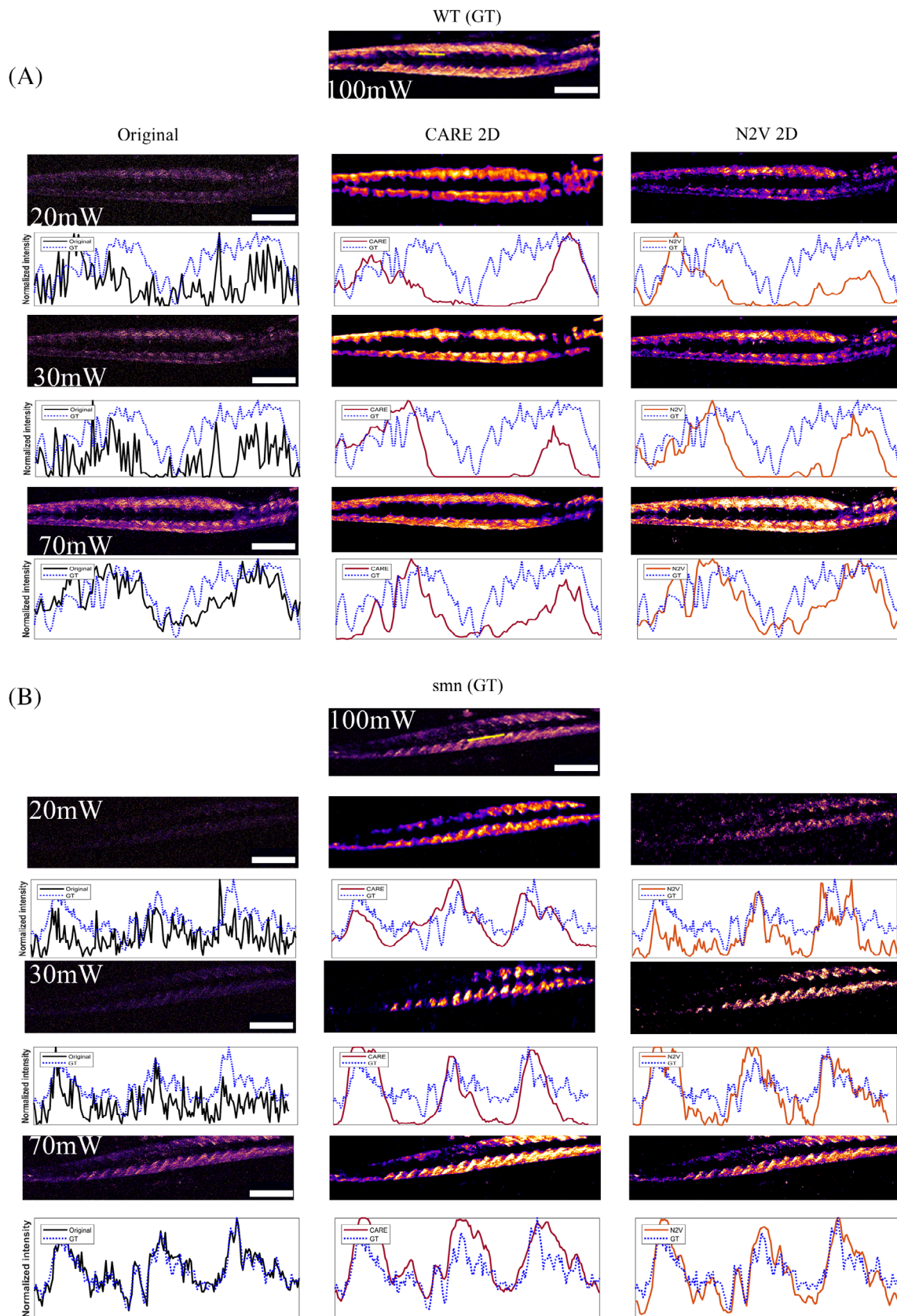


**FIGURE 6** (A) Wild-type (WT) and (B) *smn*<sup>-/-</sup> fish along their intensity profiles from a random region of interest (ROI). The ROI was identical across all samples. The legends correspond to the original structure (black solid line), GT (blue dotted line), CARE (red solid line), and N2V (orange solid line). The scale bar for all images is 200  $\mu\text{m}$ .

TABLE 2 mSSIM and PSNR metric for CARE 2D and N2V 2D models applied to different zebrafish strains.

Laser power (mW)	Model	Sample type	Original vs. GT mSSIM	Denosed vs. GT mSSIM	Original vs. GT PSNR (dB)	Denosed vs. GT PSNR (dB)
20	CARE	WT	0.07	0.58	17.38	21.03
30	CARE	WT	0.15	0.56	17.7	20
70	CARE	WT	0.44	0.66	19.96	22.67
20	N2V	WT	0.07	0.44	17.37	19.87
30	N2V	WT	0.15	0.5	17.7	20.24
70	N2V	WT	0.44	0.6	19.96	21.26
20	CARE	smn	0.04	0.36	18.66	20.84
30	CARE	smn	0.05	0.29	18.71	20.19
70	CARE	smn	0.22	0.39	19.68	21.51
20	N2V	smn	0.04	0.15	18.66	19.33
30	N2V	smn	0.05	0.27	18.71	20.44
70	N2V	smn	0.22	0.39	19.68	21.49

model and the original signal in terms of the intensity value while following the patterns of the original image signal. For the *smn*-/- samples, CARE 2D excels at producing the same intensity profile as the GT image at 20 mW. However, for the other samples, CARE 2D overshoots the intensity values, and N2V 2D performs better at fitting the intensity pattern of the denoised image to the GT image.

The mSSIM and PSNR metrics of the CARE 2D and N2V 2D models are summarized in Table 2.

From Table 2, we can see a significant improvement across the board, and all predicted images are better than their original counterparts, as reflected in the mSSIM and PSNR metrics. However, the loss of detail in the muscle structure is visually evident in Figure 6.

To summarize, both CARE 2D and N2V 2D successfully reduced the noise in low-SNR SHG images. However, CARE 2D often outperforms N2V 2D when laser power is a major constraint, enabling details even at very low-power settings, as demonstrated in our mammary gland images (Figure 5). While this holds true for mammary gland tissue, N2V 2D may better retain intricate details such as striated muscle fibers in zebrafish when image noise is less severe (Figure 6). These nuanced denoising outcomes across tissue types suggest that while CARE 2D excels with more homogenous patterns of stromal tissues, N2V's self-supervised learning is advantageous for handling diverse and variable patterns in muscular tissues. This observation is supported by the visual distinction in the muscle structure preserved by N2V, indicating its ability to maintain important biological details that are not fully captured by traditional metrics such as mSSIM and PSNR. The variability in performance can be tied to the representativeness of the

training data, adaptability of the algorithms to different noise distributions, and different tissues.

## 4 | CONCLUSION

Although deep learning image restoration has been explored in the context of SHG microscopy, our study provides novel insights by directly comparing the performance of CARE 2D and N2V 2D on SHG collagen and myosin images, revealing their tissue-specific strengths and weaknesses. Deep learning in image restoration has gained traction over the past few years but has not yet been thoroughly applied to SHG microscopy. SHG microscopy relies on many parameters for high-quality imaging [5], which can be tedious and time-consuming in some scenarios. As demonstrated here, deep learning image restoration can be an alternative solution to enhance SHG imaging during post-processing. Our study highlights the importance of considering a sample's specific characteristic when choosing a denoising method. CARE 2D and N2V 2D are powerful models used in image restoration that work with (CARE 2D) and without (N2V) high-quality reference images [25, 26].

We found that the glycerol concentration during fixation can lead to noisy images. At higher glycerol concentrations, N2V 2D can be used to restore SHG images despite this additional noise. Therefore, deep learning image restoration opens the possibility of fixing the significant noise and image deterioration caused by fixation chemicals. In addition, it can reduce the number of animal sacrifices required for sample preparation. Another crucial experimental aspect of SHG imaging of bio-samples is limiting the input laser power to reduce the

possibility of sample damage at the cost of image SNR. This 70% decrease in the input laser power is also particularly useful for shifting the imaging from fixed to live samples. Moreover, at 30 mW, we can see the full layout of the structure at 110 mW. Given that the SHG signal is quadratically proportional to the input laser power, the input power can be significantly reduced using deep learning without loss in the SHG signal.

The nuanced denoising outcomes for 2D and N2V CARE across tissue types demonstrate their unique capabilities. While CARE 2D excels with more homogenous patterns of stromal tissues owing to its training on well-represented datasets, it can sometimes lead to over-smoothing, obscuring fine details. N2V's self-supervised learning, on the other hand, allows it to maintain important structural nuances in tissues with variable patterns like muscle, even if this approach sometimes results in lower quantitative metrics. This observation is supported by the visual distinction in the muscle structure preserved by N2V, indicating its ability to maintain important biological details that are not fully captured by traditional metrics such as mSSIM and PSNR. The variability in performance can be tied to the representativeness of the training data and adaptability of the algorithms to different noise distributions. A hybrid approach that combines reference-based learning of CARE 2D with the self-learning capabilities of N2V could potentially harness the strengths of both methods, leveraging CARE 2D's structure-preserving capabilities in consistent-pattern tissues while utilizing N2V's detail-retaining flexibility in variable-pattern tissues. An algorithm trained to classify tissue types can enable dynamic switching between CARE 2D and N2V 2D based on image characteristics, providing a more robust and versatile denoising approach.

Future research directions could include developing an adaptive framework that initially classifies tissue types and then applies the most suitable denoising techniques. Machine learning algorithms can be deployed to dynamically select between CARE 2D and N2V 2D based on the visual and noise characteristics of the tissue, potentially guided by an ensemble of metrics that include both traditional scores and assessments of structural fidelity. In summary, the optimal denoising strategy may vary not only with the tissue type but also with the specific structural features and noise characteristics present in the SHG images. Balancing quantitative assessment with qualitative visual analysis is essential to advance the application of deep learning in SHG imaging denoising. Looking ahead, we envision a composite model that synergizes CARE 2D's structural precision with N2V 2D flexible adaptation to varied noise profiles governed by real-time, sample-specific algorithmic decisions. This

paradigm shift necessitates the construction of comprehensive datasets, fostering model generalization across SHG applications. The broader implications of our work suggest a transformative impact on live imaging methodologies, advocating minimal laser usage to preserve the sample integrity. Ultimately, this study lays foundational groundwork, steering future explorations toward more sophisticated and versatile imaging solutions.

## FUNDING INFORMATION

The authors acknowledge financial support from the Canada Foundation for Innovation, Fonds de recherche du Québec–Nature et Technologies, the Natural Sciences and Engineering Research Council of Canada, and the New Frontiers Research Fund. Arash Aghigh thanks the NSERC CREATE program for the scholarship. Canadian Cancer Society (grant #707140 to Sonia V. Del Rincón). Samuel E. J. Preston was supported by a doctoral fellowship from Fonds de Recherche Québec Santé (FRQS) and the Epstein Fellowship in Women's Health (Faculty of Medicine, McGill University).

## CONFLICT OF INTEREST STATEMENT

The authors declare that they have no conflicts of interest.

## DATA AVAILABILITY STATEMENT

Data underlying the results presented in this paper are not publicly available at this time but may be obtained from the authors upon reasonable request.

## ORCID

Arash Aghigh  <https://orcid.org/0000-0001-6205-4707>

Melika Saadat Mohammadi  <https://orcid.org/0009-0008-4732-2142>

## REFERENCES

- [1] A. Aghigh, S. Bancelin, M. Rivard, M. Pinsard, H. Ibrahim, F. Légaré, *Biophys. Rev* **2023**, *15*, 43.
- [2] D. S. James, P. J. Campagnola, *BME Front.* **2021**, *2021*, 3973857.
- [3] G. Borile, D. Sandrin, A. Filippi, K. I. Anderson, F. Romanato, *Int. J. Mol. Sci.* **2021**, *22*, 2657.
- [4] H. Yokota, J. Kaneshiro, Y. Uesu, *Phys. Res. Int.* **2012**, *2012*, e704634.
- [5] E. E. Hoover, J. A. Squier, *Nat. Photonics* **2013**, *7*, 93.
- [6] G. H. Patterson, D. W. Piston, *Biophys. J.* **2000**, *78*, 2159.
- [7] K. König, P. T. C. So, W. W. Mantulin, E. Gratton, *Opt. Lett.* **1997**, *22*, 135.
- [8] K. König, H. Liang, M. W. Berns, B. J. Tromberg, *Nature* **1995**, *377*, 20.
- [9] X. Chen, O. Nadiarynk, S. Plotnikov, P. J. Campagnola, *Nat. Protoc.* **2012**, *7*, 654.
- [10] S. V. Plotnikov, A. C. Millard, P. J. Campagnola, W. A. Mohler, *Biophys. J.* **2006**, *90*, 693.

- [11] V. Van Steenbergen, W. Boesmans, Z. Li, Y. de Coene, K. Vints, P. Baatsen, I. Dewachter, M. Ameloot, K. Clays, P. Vanden Berghe, *Nat. Commun.* **2019**, *10*, 3530.
- [12] G. Wang, H. Zhan, T. Luo, B. Kang, X. Li, G. Xi, Z. Liu, S. Zhuo, *IEEE J. Sel. Top. Quantum Electron.* **2023**, *29*, 1.
- [13] A. E. Woessner, K. P. Quinn, *J. Biophotonics* **2022**, *15*, e202200191.
- [14] R. Houhou, E. Quansah, T. Meyer-Zedler, M. Schmitt, F. Hoffmann, O. Guntinas-Lichius, J. Popp, T. Bocklitz, *Biomed. Opt. Express* **2023**, *14*, 3259.
- [15] A. Fast, A. Lal, A. F. Durkin, G. Lentsch, R. M. Harris, C. B. Zachary, A. K. Ganesan, M. Balu, *Sci. Rep.* **2020**, *10*, 18093.
- [16] C. Belthangady, L. A. Royer, *Nat. Methods* **2019**, *16*, 1215.
- [17] Z. Liu, L. Jin, J. Chen, Q. Fang, S. Ablameyko, Z. Yin, Y. Xu, *Comput. Biol. Med.* **2021**, *134*, 104523.
- [18] M. E. Helou, S. Süssstrunk, *IEEE Trans. Image Process* **2022**, *31*, 1628.
- [19] C. Qiao, D. Li, Y. Guo, C. Liu, T. Jiang, Q. Dai, D. Li, *Nat. Methods* **2021**, *18*, 194.
- [20] C. Qiao, D. Li, Y. Liu, S. Zhang, K. Liu, C. Liu, Y. Guo, T. Jiang, C. Fang, N. Li, Y. Zeng, K. He, X. Zhu, J. Lippincott-Schwartz, Q. Dai, D. Li, *Nat. Biotechnol.* **2022**, *1–11*. <https://doi.org/10.1038/s41592-020-01048-5>
- [21] L. Jin, B. Liu, F. Zhao, S. Hahn, B. Dong, R. Song, T. C. Elston, Y. Xu, K. M. Hahn, *Nat. Commun.* **2020**, *11*, 1934.
- [22] H. Wieslander, C. Wählby, I.-M. Sintorn, *PLoS One* **2021**, *16*, e0246336.
- [23] T.-O. Buchholz, A. Krull, R. Shahidi, G. Pigino, G. Jékely, F. Jug, in *Methods in Cell Biology*, Vol. 152 (Eds: T. Müller-Reichert, G. Pigino), Academic Press, Cambridge, Massachusetts **2019**, p. 277. Three-Dimensional Electron Microscopy.
- [24] J. Lehtinen, J. Munkberg, J. Hasselgren, S. Laine, T. Karras, M. Aittala, and T. Aila, “Noise2Noise: Learning Image Restoration without Clean Data,” Cornell University, Ithaca, NY (2018).
- [25] A. Krull, T.-O. Buchholz, and F. Jug, “Noise2Void—Learning Denoising from Single Noisy Images,” (2019).
- [26] M. Weigert, U. Schmidt, T. Boothe, A. Müller, A. Dibrov, A. Jain, B. Wilhelm, D. Schmidt, C. Broaddus, S. Culley, M. Rocha-Martins, F. Segovia-Miranda, C. Norden, R. Henriques, M. Zerial, M. Solimena, J. Rink, P. Tomancak, L. Royer, F. Jug, E. W. Myers, *Nat. Methods* **2018**, *15*, 1090.
- [27] O. Ronneberger, P. Fischer, and T. Brox, “U-Net: Convolutional Networks for Biomedical Image Segmentation,” Cornell University, Ithaca, NY (2015).
- [28] D. Rouse, S. Hemami, 2008 15th IEEE International Conference on Image Processing, IEEE Xplore in Piscataway, New Jersey **2008**, p. 1188.
- [29] Z. Wang, A. C. Bovik, H. R. Sheikh, E. P. Simoncelli, *IEEE Trans. Image Process.* **2004**, *13*, 600.
- [30] V. Mudeng, M. Kim, S. Choe, *Appl. Sci.* **2022**, *12*, 3754.
- [31] A. Horé, D. Ziou, 2010 20th International Conference on Pattern Recognition, 2010, IEEE Xplore in Piscataway, New Jersey p. 2366.
- [32] M. Westerfield, *THE ZEBRAFISH BOOK, 5th Edition; A guide for the laboratory use of zebrafish (Danio rerio)*. University of Oregon Press, Eugene **2007**. Paperback.
- [33] C. B. Kimmel, W. W. Ballard, S. R. Kimmel, B. Ullmann, T. F. Schilling, *Dev. Dyn* **1995**, *203*, 253.
- [34] G. J. Espinoza, J. M. Poland, J. R. A. Bremer, *BioTechniques* **2017**, *63*, 181.
- [35] L. von Chamier, R. F. Laine, J. Jukkala, C. Spahn, D. Krentzel, E. Nehme, M. Lerche, S. Hernández-Pérez, P. K. Mattila, E. Karinou, S. Holden, A. C. Solak, A. Krull, T.-O. Buchholz, M. L. Jones, L. A. Royer, C. Leterrier, Y. Shechtman, F. Jug, M. Heilemann, G. Jacquemet, R. Henriques, *Nat. Commun* **2021**, *12*, 2276.
- [36] M. D. Bloice, P. M. Roth, A. Holzinger, *Bioinformatics* **2019**, *35*, 4522.
- [37] L. Silvestri, I. Costantini, L. Sacconi, F. S. Pavone, *J. Biomed. Opt* **2016**, *21*, 081205.
- [38] M. J. Anzanello, F. S. Fogliatto, *Int. J. Ind. Ergon* **2011**, *41*, 573.
- [39] N. Srivastava, G. Hinton, A. Krizhevsky, I. Sutskever, R. Salakhutdinov, *J. Mach. Learn. Res* **2014**, *15*, 1929.

**How to cite this article:** A. Aghigh, G. Jargot, C. Zaouter, S. E. J. Preston, M. S. Mohammadi, H. Ibrahim, S. V. Del Rincón, K. Patten, F. Légaré, *J. Biophotonics* **2024**, e202300565. <https://doi.org/10.1002/jbio.202300565>